Phosphotyrosine-mediated LAT assembly on membranes drives kinetic bifurcation in recruitment dynamics of the Ras activator SOS

William Y. C. Huang[a], Qingrong Yan[b,c], Wan-Chen Lin[a], Jean K. Chung[a], Scott D. Hansen[a], Sune M. Christensen[a], Hsiung-Lin Tu[a,1], John Kuriyan[a,b,c], and Jay T. Groves[a,2]

[a]Department of Chemistry, University of California, Berkeley, CA 94720; [b]Howard Hughes Medical Institute, University of California, Berkeley, CA 94720; and [c]Department of Molecular and Cell Biology, University of California, Berkeley, CA 94720

Edited by Michael L. Klein, Temple University, Philadelphia, PA, and approved May 17, 2016 (received for review March 18, 2016)

The assembly of cell surface receptors with downstream signaling molecules is a commonly occurring theme in multiple signaling systems. However, little is known about how these assemblies modulate reaction kinetics and the ultimate propagation of signals. Here, we reconstitute phosphotyrosine-mediated assembly of extended linker for the activation of T cells (LAT):growth factor receptor-bound protein 2 (Grb2):Son of Sevenless (SOS) networks, derived from the T-cell receptor signaling system, on supported membranes. Single-molecule dwell time distributions reveal two, well-differentiated kinetic species for both Grb2 and SOS on the LAT assemblies. The majority fraction of membrane-recruited Grb2 and SOS both exhibit fast kinetics and single exponential dwell time distributions, with average dwell times of hundreds of milliseconds. The minor fraction exhibits much slower kinetics, extending the dwell times to tens of seconds. Considering this result in the context of the multistep process by which the Ras GEF (guanine nucleotide exchange factor) activity of SOS is activated indicates that kinetic stabilization from the LAT assembly may be important. This kinetic proofreading effect would additionally serve as a stochastic noise filter by reducing the relative probability of spontaneous SOS activation in the absence of receptor triggering. The generality of receptor-mediated assembly suggests that such effects may play a role in multiple receptor proximal signaling processes.

signal transduction | protein assembly | kinetic proofreading | membrane dwell time | single molecule

Assembly of receptors with adaptor proteins and effectors has been well documented in multiple signal transduction systems. Some examples include the growth factor receptors (1, 2), components pertaining to actin cytoskeleton reorganization (3), Ephrin receptors (4–9), and membrane receptors in T cells (10–12). In each of these systems, the signaling molecules contain repetitive multivalent protein–protein interaction domains that drive the extended assembly of molecular complexes during signal transduction. Tyrosine phosphorylation is a prototypical mediator of such assembly.

In the case of T-cell receptor (TCR) signaling, linker for the activation of T cells (LAT) has several tyrosines (Y) that are phosphorylated upon TCR triggering. Three of these (Y171, Y191, and Y226) are known to recruit the cytosolic adaptor protein, growth factor receptor-bound protein 2 (Grb2), by its SH2 domain (13). Grb2 additionally has two SH3 domains, which bind to the proline-rich regions in the C-terminal domain of the nucleotide exchange factor, Son of Sevenless (SOS) (14). A single SOS molecule can associate with at least two Grb2 molecules (15), enabling the LAT:Grb2:SOS interactions to form an extended network assembly on membranes upon LAT phosphorylation (15–18) (Fig. 1). Similar assemblies have been reconstituted in vitro for the nephrin:Nck:N-WASP system on 2D membrane surfaces (3, 19). In live cells, introduction of mutations that reduce the multivalency in the LAT:Grb2:SOS assembly alter the spatial pattern of the receptors (15, 20) and disrupt the downstream signaling (21, 22). Although the existence of these signaling assemblies is documented, the physical mechanisms by which they modulate signal transduction remain unclear.

Because assembly intrinsically involves increasing the local concentration of molecules, it is often thought that this increased concentration will lead to enhanced reaction kinetics and therefore facilitate signal propagation. However, this conclusion is based on the assumption that dynamical parameters of the system, such as molecular binding kinetics and diffusive mobility, are unchanged in the condensed structure. In fact, we would expect such dynamical parameters to be strongly modulated by assembly—thus offering various possibilities for the ways assembly may enhance, inhibit, or conceivably redirect signaling. Actual quantitative measurements of such kinetic properties are sparse (20, 23, 24). Here, we reconstitute phosphotyrosine-mediated LAT:Grb2:SOS assembly on supported membranes with the purpose of performing a quantitative analysis of how the extended network assembly influences the molecular kinetics of Grb2 and SOS recruitment.

Measurements of single-molecule binding dwell time distributions reveal two, well-differentiated kinetic species for both Grb2 and SOS on LAT assemblies. The majority fraction of membrane-recruited Grb2 and SOS both exhibit fast single exponential kinetics, with average dwell times of hundreds of milliseconds. These kinetics are nearly identical with those observed in the unassembled state and thus correspond to monovalent binding interactions. A subpopulation of the molecules, however, exhibits much slower binding kinetics, with dwell times extending to tens of seconds.

Significance

The assembly of receptors and downstream signaling molecules into extended networks is a commonly observed phenomenon in signal transduction. However, little is known about how such assemblies physically modulate signal propagation. Here, based on single-molecule kinetics studies, we report that phosphotyrosine-mediated assembly of adaptor protein LAT networks yields two distinct kinetic species of the Ras activator SOS. This system regulates the transmission of signal from activated T-cell receptor to Ras. We propose and evaluate how the emergence of a long-dwelling SOS species may serve as a kinetic proofreading mechanism to discriminate stochastic noise from genuinely activated receptors.

Author contributions: W.Y.C.H., Q.Y., J.K., and J.T.G. designed research; W.Y.C.H., W.-C.L., J.K.C., and H.-L.T. performed research; Q.Y., S.D.H., and S.M.C. contributed new reagents/analytic tools; W.Y.C.H. analyzed data; and W.Y.C.H. and J.T.G. wrote the paper.

The authors declare no conflict of interest.

This article is a PNAS Direct Submission.

[1]Present address: Department of Biosystems Science and Engineering, Eidgenössische Technische Hochschule Zürich, Basel, 4058 Switzerland.

[2]To whom correspondence should be addressed. Email: jtgroves@lbl.gov.

This article contains supporting information online at www.pnas.org/lookup/suppl/doi:10.1073/pnas.1602602113/-/DCSupplemental.

www.pnas.org/cgi/doi/10.1073/pnas.1602602113

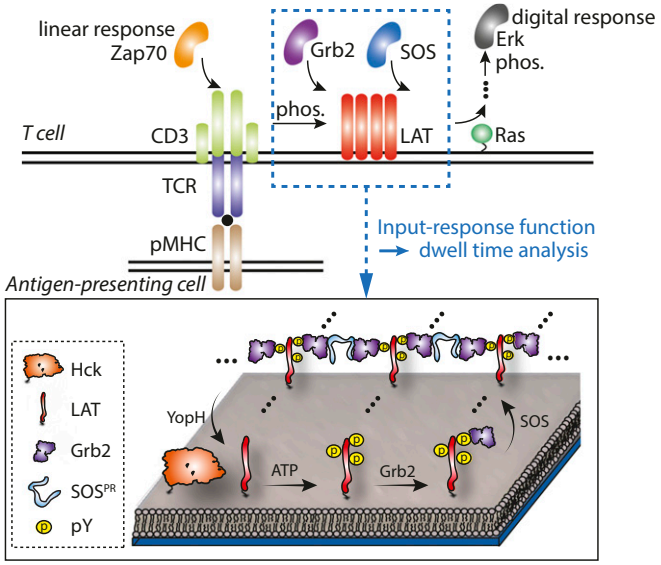

Fig. 1. Quantification of the input-response function of LAT:Grb2:SOS assembly in TCR signaling. Schematic of TCR signaling pathway (*Top*) and the in vitro-reconstituted system (*Bottom*). Engagement of TCR with pMHC results in phosphorylation of LAT, which triggers assembly reaction on the cytoplasmic side of the plasma membrane. LAT assembly promotes SOS membrane recruitment and activation, which propagates downstream signals. To quantitatively assess the input-response function at the LAT signaling node, the signaling geometry of LAT is reconstituted on supported membranes. Phosphorylation of LAT is triggered by membrane-bound tyrosine kinase Hck, which results in Grb2 recruitment. The assembly reaction is initiated by the addition of SOS proline-rich domain and can be reversed by tyrosine phosphatase, YopH.

These long-lived Grb2 and SOS binding events arise from multivalent interactions within the LAT:Grb2:SOS assembly.

Activation of the Ras GEF (guanine nucleotide exchange factor) activity of full-length SOS involves a multistep process (25). Following membrane recruitment by Grb2, structural rearrangements within SOS expose lipid-binding domains that stabilize the protein on the membrane, expose the allosteric Ras-binding site, and release autoinhibition of SOS guanine nucleotide exchange activity. Once fully activated, SOS remains on the membrane and processively catalyzes nucleotide exchange on many Ras molecules (26). Because SOS activation requires a sequence of events, its activation is subject to a type of kinetic proofreading (27, 28), by which molecules that dwell on the membrane for longer periods of time are disproportionately more likely to become activated. A corollary of this fact is that for the same total amount of membrane recruited SOS, more SOS molecules will become activated if a slow kinetic species exists—or in the extreme case, only the slow kinetic species activate. The slow kinetic species of membrane recruited SOS, which is here uniquely observed in phosphotyrosine-mediated LAT assemblies, could thus correspond to the activating condition for this molecule. This kinetic proofreading would have the effect of limiting SOS activation to regions of genuine receptor triggering and the resultant LAT assembly, while reducing the probability of spontaneous SOS activation elsewhere on the cell membrane. The generality of this type of kinetic proofreading suggests that such a mechanism may be at play in multiple receptor proximal signaling processes.

Results

Phosphotyrosine-Mediated LAT:Grb2:SOS Assembly on Supported Membranes. In the following experiments, the cytoplasmic domain (residues 30–233) of LAT is purified with an N-terminal His_6 tag and chemically modified with a maleimide fluorophore (Alexa Fluor 555) at cysteine 146 (with a labeling efficiency of 60%). This His_6-LAT, here referred to as LAT, can be stably linked to supported membranes containing Ni-NTA lipids (4 mol%) (29). The membrane associated LAT is laterally diffusive, as characterized by fluorescence recovery after photobleaching (FRAP) experiments and single-particle tracking (SPT) (Fig. S1). A single diffusive population with diffusion coefficients of ~1.8 $\mu m^2/s$ (Fig. S1) is typically observed, indicating that LAT behaves as a monomeric molecule on supported membranes (30). Surface densities of LAT can be controlled from 100 to 5,000 molecules per square micron and were calibrated by fluorescence correlation spectroscopy (FCS) (Fig. S2). In these experiments, LAT is phosphorylated by membrane-tethered Src family kinase Hck (Fig. S3). The phosphorylation reaction is monitored by the membrane recruitment of full length Grb2 coupled to a fluorophore (Alexa Flour 647) using maleimide-thiol chemistry at Cysteine 32 (with a labeling efficiency of 95%). On a total internal reflection fluorescence (TIRF) microscope, Grb2 recruitment reports the phosphorylation of LAT in real time; LAT:Grb2 exhibits relatively fast binding kinetics (k_{-1} = 1.5 s^{-1}) compared with the phosphorylation reaction (~1–2 min) (Fig. S3). Other kinases, including Zap70 (31), can also be used to phosphorylate LAT without appreciable differences detectable by Grb2 binding (Fig. S4).

A macroscopic network assembly of phosphorylated LAT (pLAT) forms on the membranes when the proline-rich domain (residues 1,051–1,333) of SOS (abbreviated as SOS) and Grb2 are both present in the solution (Figs. 1 and 2*A* and Movie S1). Assembly depends on the solution concentrations of Grb2, SOS and the membrane surface density of pLAT (Fig. S5). Using 5.8 μM Grb2 and 1.45 μM SOS (the ratio of the concentrations for Grb2 and SOS is fixed to 4 for all experiments) over a pLAT density of about 2,400 molecules per square micron, small mobile puncta of highly dense LAT emerged across the membrane within 3 min of mixing (red arrow in Fig. 2*A*). These initial pLAT assemblies subsequently evolve into a macroscopic protein-dense phase (with an estimated density of ~4,000 molecules per square micron) that is interspersed with regions devoid of LAT (Fig. 2*A* and Movie S1). The assembly is dynamic; FRAP measurements on LAT reveal recovery of intensity in photobleached spots (diameter, 21 μm; τ_D = 704 s; $D_{effective}$ = 0.20 $\mu m^2/s$) (Fig. S6). The assembly is governed by multiple tyrosine phosphorylation of LAT, as confirmed by the following observations. (*i*) Kinase-dependent LAT phosphorylation is required for assembly formation (Fig. S7). (*ii*) LAT mutants containing only a single Grb2 accessible phosphotyrosine site fail to form the assembly under the same experimental conditions (Fig. S7). (*iii*) Introduction of a tyrosine phosphatase (10 μM YopH) in the solution rapidly reverses this entire process, within a minute (Fig. 2*B* and Movie S2), eliminating Grb2 recruitment to LAT (Fig. S7) and driving the system back to a uniform and fluid distribution of LAT on the membrane. FRAP experiments on LAT before assembly and after dephosphorylation reveal similar free mobilities, with τ_D values of 113 s (D = 1.26 $\mu m^2/s$) and of 115 s (D = 1.24 $\mu m^2/s$), respectively (Fig. S6).

This type of phosphotyrosine-mediated condensation and assembly resembles a gelation phase transition (3, 19). Theoretical studies of the LAT:Grb2:SOS system specifically predict the existence of a gelation phase transition (16). Leaving the details of whether or not the condensed phase experimentally observed here meets the technical definition of a gel phase (32) to a later discussion, the transition itself is empirically discrete. We experimentally map its effective phase diagram as a function of LAT, Grb2, and SOS concentrations. (Fig. S5). The assemblies can form with a LAT density as low as ~600 molecules per square micron. Macroscopic features of the condensed phase, such as the domain size, geometric distribution, and fractional area coverage can be

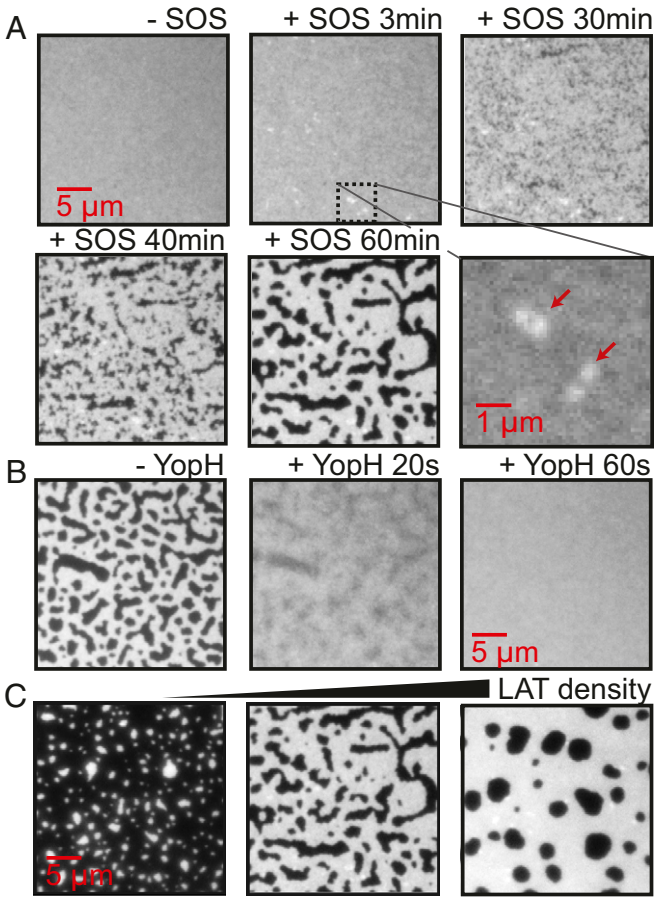

Fig. 2. LAT:Grb2:SOS is sufficient to drive an assembly network on membrane surfaces. (*A*) Epifluorescence images of LAT undergoing an assembly reaction. After injection of 5.8 μM Grb2 and 1.45 μM SOS, small puncta of densely assembled proteins (red arrow) appear within a few minutes. The emergence of a macroscopic protein-dense phase was observed after 30 min. (*B*) Reversibility of the assembly. The phase boundary disintegrated abruptly into a homogenous phase after incubation of 10 μM phosphatase YopH. (*C*) Different geometries and sizes of LAT assemblies by manipulating the surface densities of LAT ranging from 600 to 4,000 molecules per square micron in the presence of 5.8 μM Grb2 and 1.45 μM SOS.

controlled by the average LAT density (Fig. 2*C*). However, intensive properties such as molecular binding kinetics should be independent of the size of LAT assembly. With single-molecule dwell time measurements on different sizes of LAT assemblies (Fig. S8), we affirm that the binding kinetics of these assemblies are not influenced by their macroscopic geometry (Fig. S8). The LAT assembly exhibits essentially the same molecular level behavior regardless of its large-scale shape and appearance. We therefore take advantage of the extended assembled structures (a few microns in size) for better spatial resolution for single-molecule measurements, as described below.

Kinetic Bifurcation of Grb2 and SOS Membrane Dwell Time from Single-Molecule Analysis. TIRF imaging of fluorescently labeled (Alexa Fluor 647) Grb2 or SOS enables observation of membrane recruitment, movement on the membrane surface, and desorption, at the single molecule level (Fig. 3*B*). Single-step photobleaching, determined unambiguously with a Bayesian algorithm (33), verified that the tracked objects were single molecules (Fig. 3*B*). In the case of simple bimolecular kinetics of pLAT:Grb2, a single population of short, exponentially distributed, dwell time is observed. The mean dwell time, 0.65 s (acquired at a framerate of 21 Hz), corresponds to an ensemble kinetic off rate ($k_{-1,\mathrm{pLAT:Grb2}}$) of 1.5 s^{-1}, after correction for the measured photobleaching rate (Fig. 3*C*, *SI Materials and Methods*, and ref. 34).

For analyses of Grb2 and SOS kinetics on the LAT:Grb2:SOS assembly, we acquire Grb2 or SOS single-molecule images during the quasi-stationary state, in which the assembly exhibits a stable geometry with only local phase boundary fluctuations (Fig. 4 and Fig. S6). The assembly produces a notable affect on the recruitment rate of Grb2. At a fixed Grb2 solution concentration of 5.8 μM and a pLAT membrane density of ~2,400 molecules per square micron, the presence of SOS (1.45 μM in solution) leads to a fivefold faster rate of Grb2 recruitment (Fig. S9). We also observe an enhancement in the membrane-bound Grb2:SOS ratio, which is >10:1 in the assembly compared with the bulk concentration ratio of 4:1. These observations were made using two-color imaging of Alexa Fluor 647-labeled Grb2 and Atto 488-labeled SOS. The enhanced recruitment could be attributed to the increased affinity of SOS-bound Grb2 to pLAT (35), the presence of membrane-bound SOS (providing more binding sites), or physical alterations in the structure and accessibility of pLAT in the assembly.

The dwell time distributions for both Grb2 and SOS are altered on the LAT assemblies. Specifically, a second kinetic species with dwell times two orders of magnitude longer for both proteins emerges (Fig. 4*A* and Movie S3). At a framerate of 2 Hz, the slow kinetic species is resolved clearly (Movie S3). Apparent dwell times of the long-lived Grb2 ranged from 10 to 100 s. Mapping trajectories of molecules with dwell times greater than 10 s reveals highly constrained motion within the network assembly (Fig. 4*C*). Furthermore, the dwell time distribution deviates from a single exponential (Fig. 4*A*), which implies that the long-dwelling species is a convolution of multiple binding states. For both Grb2

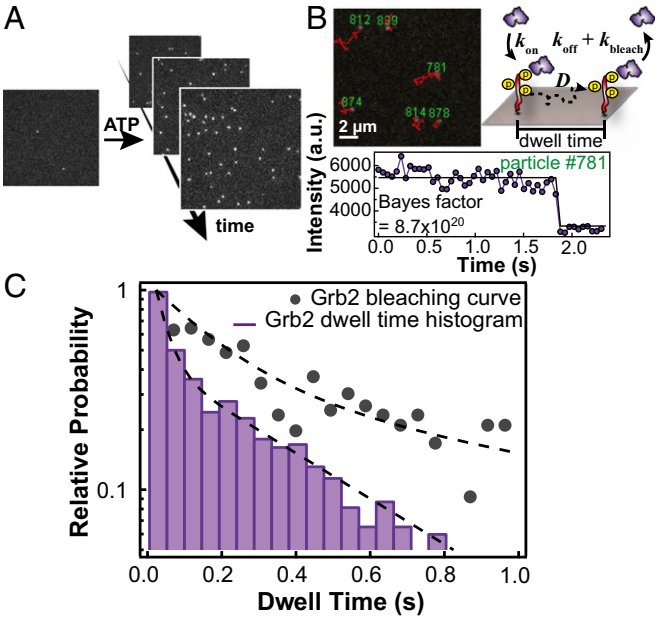

Fig. 3. Input-response function parameterized by single-molecule dwell time analysis. (*A*) Single-molecule images showing the gradual increase in Grb2 recruitment following LAT phosphorylation. (*B*) Diffusion and dissociation kinetics for membrane recruited Grb2 measured from single-particle tracking. Single-step photobleaching confirmed that the tracked Grb2 is a single molecule. The existence of a change point was detected using a Bayesian algorithm. (*C*) Dwell time histogram of Grb2 (purple histogram). After correction of photobleaching (black dots), the dwell time of LAT:Grb2 is 0.65 ± 0.10 s, setting the baseline of the input-response function before any assembly structure. Dashed line is fitting to a single kinetic population (Eq. S2).

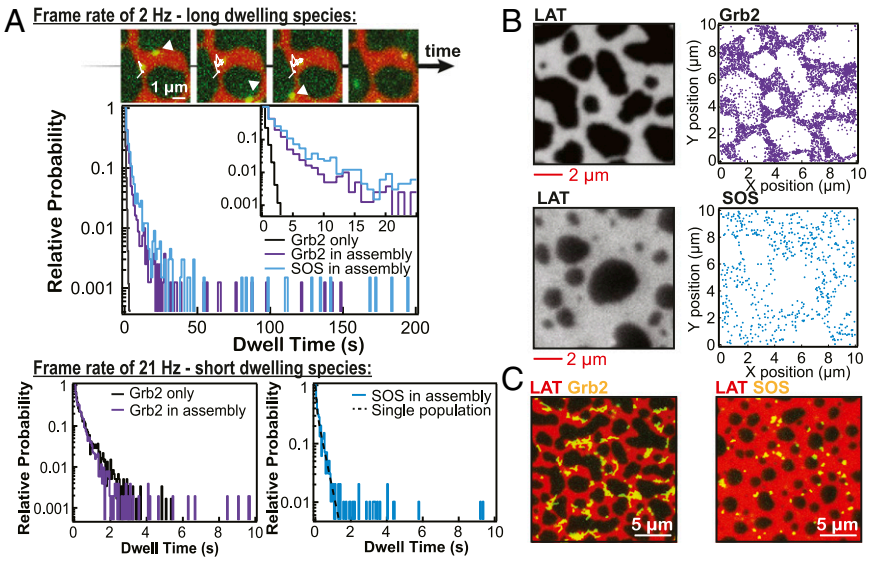

Fig. 4. Protein assembly creates kinetic bifurcation in the recruitment dynamics of Grb2 and SOS. (*A*) The kinetic species of interest are evaluated at the two different frame rates of 2 and 21 Hz. The top lane shows the time-lapse imaging of Grb2 and SOS at the framerate of 2 Hz. The assembly structure is marked by labeled LAT (red). Membrane-bound Grb2 (yellow) exhibits two kinetic populations: short dwell times (white arrow) and long dwell times (white tracks). The statistics are summarized in the dwell time histograms: Grb2 before assembly structure (black), Grb2 in protein assembly (purple), and SOS in protein assembly (blue). The bottom row shows dwell time histogram of Grb2 and SOS in protein assembly acquired at the framerate of 21 Hz. The fast kinetic species of Grb2 in protein assembly (purple) exhibits identical rate as the binding kinetics of pLAT:Grb2 before assembly (black). The fast kinetic species of SOS (blue) is also well described by a single kinetic population, with a fitted $k_{app,SOS}$ of 3.4 s^{-1}. (*B*) Grb2 and SOS are recruited to the LAT assembly. Strong correlations are observed between epifluorescence images of LAT (*Left*) and the reconstructed images of Grb2 (*Top Right*) and SOS (*Lower Right*), obtained by compiling all single-molecule recruitment events within 400 s. (*C*) By mapping trajectories with apparent dwell time greater than 10 s onto the LAT patterns, it is evident that the long-dwelling species localize to the assembly structure.

and SOS, the long-lived species represents only a minor fraction (population fraction, <0.1) of the total amount of membrane recruited protein; the majority fraction still exhibits fast kinetics. At a framerate of 21 Hz, the fast kinetic species is clearly resolved and proves to be identical to that of the monovalent binding kinetics of pLAT:Grb2 described above (Fig. 4*A*).

The long-lived SOS species exhibits longer dwell times than those observed for Grb2 ($\langle\tau_{SOS}\rangle \sim 29.3$ s, $\langle\tau_{Grb2}\rangle \sim 10.8$ s, estimated from trajectories with an apparent dwell time greater than 3 s) (Fig. 4*A*). This mismatch in dwell time indicates that Grb2 and SOS are not in a stable complex on the membrane over the time scale of seconds. Instead, the molecules must undergo dissociation and rebinding processes in the assembly such that the long-dwelling SOS species interacts with multiple membrane-bound Grb2. Incidentally, the time scale of the long-lived SOS is comparable to the slow transition rate between different active SOS conformations observed in single-molecule studies of SOS activation of Ras (26, 36). The majority fraction of recruited SOS also exhibits fast kinetics (Fig. 4*A*), although comparison with the monovalent binding kinetics of Grb2:SOS is unlike the simple case of pLAT:Grb2. Nonetheless, by assuming that the fast kinetic species corresponds to the monovalent interaction, we estimate $k_{-1,Grb2:SOS} = 0.47\ s^{-1}$ from $k_{app,SOS} = k_{-1,Grb2:LAT} + k_{-1,Grb2:SOS} + k_{bl,SOS}$, where $k_{app,SOS}$ is the apparent dissociation rate and $k_{bl,SOS}$ is the photobleaching rate.

Discussion

Single-molecule dwell time analysis reveals two, well-differentiated kinetic species of Grb2 and SOS in the LAT:Grb2:SOS assembly. The fast kinetic species corresponds to the monovalent interaction, whereas the long-dwelling species stems from multivalent engagement within the networked assembly. Motivated by these observations, we then ask whether the elongation of dwell times can have a qualitatively different functional consequence, specifically in terms of the activation probability of the recruited effectors. More broadly, can kinetic stabilization from protein assembly be used by biochemical networks to distinguish genuine receptor-triggered signals from molecular stochastic noise? If so, what are the mechanistic requirements? We evaluate these questions analytically in the following by considering the activation process of SOS on the membrane surfaces.

Control of SOS activity on membranes is multilayered (25, 37). After Grb2-dependent membrane recruitment, SOS activation requires the release of autoinhibition, which involves conformational changes to expose lipid-binding domains and the engagement of Ras at the allosteric binding pocket of SOS. This multistep process all but guarantees the existence of one or more kinetics intermediates. It is thus natural to presume that a finite amount of time is required for SOS to be fully activated following initial membrane recruitment. From the single-molecule point of view (38, 39), SOS (or any other cytosolic enzyme) can be defined to reach activation on the membrane at time t if (i) it is still bound to the membrane at time t and (ii) it advances through all kinetic intermediates at time t (Fig. 5*A*). Considering dissociation as a Poisson process parameterized by a rate constant k_{-1}, the probability density of activation on the membrane, $p(t)$, can be expressed as:

$$p(t) = e^{-k_{-1}t} \cdot p_N(t), \qquad [1]$$

where $p_N(t)$ is the distribution of activation time for N kinetic intermediates. Progression through a series of N kinetic intermediates can be described as a series of Poisson processes, with kinetic rates $\{k_1, k_2, \ldots, k_N\}$ for the N intermediates and k_A for the final activation step (Fig. 5*A*), such that $p_N(t)$ is the successive convolution of the lifetime probability distribution at each step:

$$p_N(t) = k_1 e^{-k_1 t} \otimes k_2 e^{-k_2 t} \otimes \ldots \otimes k_N e^{-k_N t} \otimes k_A e^{-k_A t}. \qquad [2]$$

Although the rate constants in this model are independent and can differ from each other, the qualitative features of $p_N(t)$ (e.g., shape of the distribution) are readily revealed in the simplifying case where individual kinetic transitions have equal rate constants, in which case $p_N(t)$ is a gamma distribution, $p_N(t) = ((N+1)k_N)^{N+1} t^N e^{-(N+1)k_N t}/N!$ (Fig. 5*B*). Note that we consider a one-parameter class of activation time distributions with constrained rate constants, i.e., transition rate constant $= (N+1)k_N$, such that the mean activation time remains identical regardless of N. This restriction allows examination of the dependence of activation rate solely on the activation mechanism instead of the activation time. Integrating $p(t)$ yields the probability to activate for a single recruitment event, P_{act}. To calibrate the strength of a kinetic

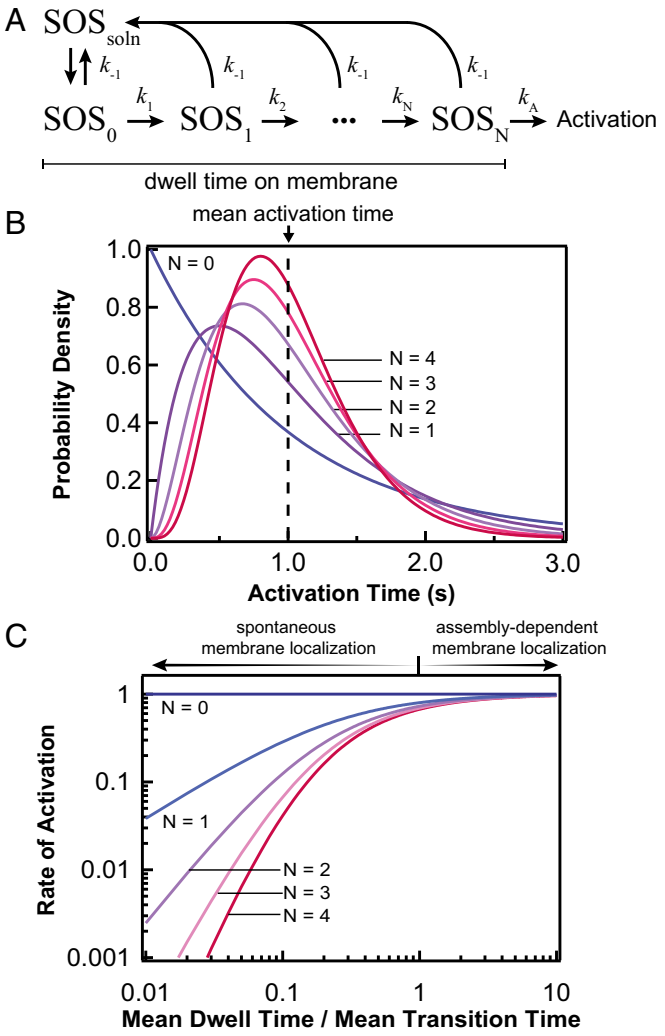

Fig. 5. Mechanistic requirements for kinetic proofreading of SOS activation on membranes. (*A*) Kinetic model for SOS activation. Following membrane recruitment of SOS, conformational transitions are required to release autoinhibition. The subscript for SOS denotes the kinetic intermediates, where N is the total number of kinetic intermediates preceding activation. k_1, k_2,..., k_N are the rate constants for the corresponding transitions of kinetic intermediates, and k_A is the activation rate constant. (*B*) The activation time distribution with different numbers of kinetic intermediates. The time dependence of activation for $n > 0$ result in the inequality of activation rates in *C*. (*C*) The rate of SOS activation as a function of the ratio between the mean dwell time and mean transition time. $k_A = 1\ s^{-1}$ in this numerical example. Short dwelling species has a lower activation rate than long-dwelling species when $n > 0$, indicating that kinetic proofreading is in play.

proofreading effects, we calculate the rate of activation, j_{act}, for a single molecule under stationary conditions:

$$j_{act} = \frac{P_{act}}{\langle \tau \rangle} = (N+1)k_A \frac{1-r}{1-r^{N+1}} r^N, \quad [3]$$

where $r = (N+1)k_N/((N+1)k_N + k_{-1})$ (*SI Materials and Methods*). This analysis is general and can describe the activation of other cytosolic enzymes on membranes.

The rate of SOS activation, j_{act}, is plotted in Fig. 5*C* as a function of the ratio of mean dwell time over mean transition time (k_N/k_{-1}). For $N = 0$, the rate of activation is identical regardless of the dwell time. In other words, when there are no kinetic intermediates en route to activation, the rate of SOS activation is proportional to the amount of membrane recruited SOS at any given time and does not depend on the dwell times for individual proteins. In this situation, kinetic proofreading is not possible. For $N > 0$, the activation rate decreases as dwell time decreases. This inequality in activation rate stems from the change in the distribution (not in the average) of the activation times, $p_N(t)$, when kinetic intermediates are involved. (Fig. 5*B*). Physically, a short dwell time does not provide sufficient time for the enzyme to restructure and reach activation. Hence to achieve kinetic proofreading for the activation of cytosolic enzymes, two requirements must be met: (*i*) elongation of dwell time and (*ii*) a multistep activation. Single-molecule and structural studies of SOS provide an estimation of the physical parameters in the model. Considering the case where the activation pathway of SOS involves two kinetic intermediates (release of autoinhibition by the N-terminal domains and engagement of Ras in the allosteric binding site) (25, 35) with slow transition rates ($N = 2$, $k_N = 0.1\ s^{-1}$) (26, 34), we estimate a 60–480 enhancement factor in the activation rate when the dwell time is elongated from 0.1 s to 1–100 s for the same total amount of membrane recruited SOS (Tables S1 and S2). Although the exact value of the parameters in cells are not known, this model allows us to estimate the potential strength of kinetic proofreading from a range of plausible parameter values (Tables S1 and S2). From the analysis, elongation of membrane dwell times of SOS in association with LAT assembly therefore implicates LAT assembly as a possible gatekeeping mechanism that limits Ras activation through kinetic proofreading in the activation of SOS (Fig. 6) The need for such restriction in SOS activation is underscored by recent single-molecule SOS:Ras activation studies, which demonstrate that a single SOS molecule is capable of processively activate thousands of Ras in a single membrane recruitment event (26).

The statistical concept of kinetic proofreading described here resembles that first proposed by Hopfield (27). A classic example of its basic implementation is found in the triggering requirement for voltage-gated ion channels (40). In the context of TCR signaling, kinetic proofreading based on multiple phosphorylation events on the TCR ITAMs in response to ligand engagement has been proposed to play a role in antigen discrimination based on

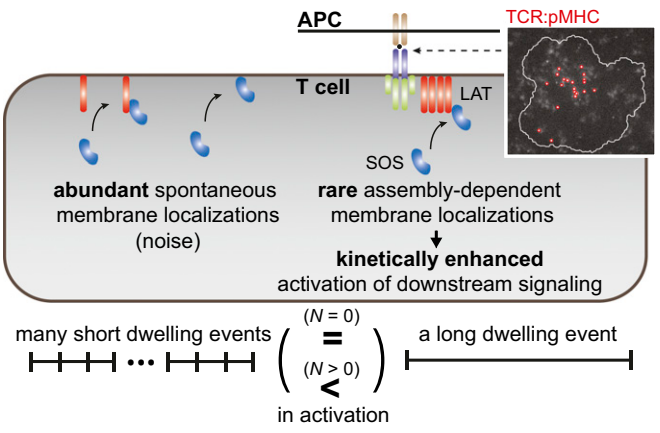

Fig. 6. Assembly-dependent membrane recruitments can achieve kinetic proofreading. Modulation of membrane dwell times can control the activation rate of cytosolic enzyme such as SOS. Kinetic proofreading of SOS ensures that receptor-dependent triggering events are distinguishable from spontaneous membrane localizations. This accuracy is especially important in TCR triggering, where detection of low agonist densities is crucial (the top right image shows that low density of TCR:pMHC complex can lead to activation). Regulation of the recruitment dynamics of biochemical networks through protein assembly thus provides a mechanism for controlling the amplification and noise filtration in signal transduction. Live cell image courtesy of Jenny J. Lin.

peptide MHC:TCR binding kinetics (19). Although the kinetic topology of SOS activation model is similar to Hopfield's, it differs slightly in two aspects: (*i*) no energy consumption is necessary, and yet a directionality of enzyme trafficking is required (a non-equilibrium process); and (*ii*) proofreading is achieved by competition between the overall activation kinetics and dissociation (Eq. **1**), instead of the kinetics of each intermediate complex.

Signal propagation in the TCR system exhibits an analog-to-digital conversion (41). Positive feedback from allosteric activation of SOS has been identified as a key element of this digitization (42). Here, we show that, before the GEF activity of SOS, LAT assembly leads to kinetic bifurcation in the recruitment dynamics of SOS, in which the activation kinetics inherently exhibit qualities necessary to enable kinetic proofreading. In addition, extension of dwell times also suggest that bifurcation in the dynamics may be a fundamental mechanism that can promote the digitization of signal transduction. Taking a broader perspective, these basic characteristics of signaling assembly and multistep activation are not unique to the TCR system, and can be found in many other systems as well including, for example EGFR:Grb2:SOS (1) and nephrin:Nck:N-WASP (3).

Materials and Methods

Protein Purification and Labeling. Human LAT cytosolic domain (residues 30–233) and full-length Grb2 were purified as described previously (43) using an N-terminal His_6 tag. Proline rich domain of SOS (residue 1,051–1,333) was purified as described in the *Supporting Information*. For Grb2 and SOS, the N-terminal His_6 tag were removed with tobacco etch virus (TEV) protease. LAT, Grb2, and SOS were labeled with Alexa Fluor 555, Alexa Fluor 647, and Alexa Fluor 647, respectively, using maleimide-thiol chemistry.

Functionalized Supported Membranes. Supported membranes were prepared from small unilamellar vesicles composed of 1,2-dioleoyl-*sn*-glycero-3-phosphocholine (DOPC) with 4 mol% 1,2-dioleoyl-*sn*-glycero-3-[(*N*-(5-amino-1-carboxypentyl)-iminodiacetic acid)succinyl] nickel salt [DGS-NTA(Ni^{2+})] lipids on piranha-etched glasses. Hck and LAT were tethered to bilayers through the nickel chelating lipids. Membrane fluidity was quantified by FRAP and SPT. Surface density of LAT was measured with fluorescence correlation spectroscopy. Assembly were triggered with Grb2 and SOS in Trolox/glucose oxidase scavenger buffer (44) and 1 mM ATP.

Fluorescence Imaging and SMT. TIRF and epifluorescence measurements were performed on a Nikon Eclipse Ti inverted microscope with a 100× 1.49 NA oil immersion TIRF objective and an iXon EMCCD (electron multiplying charge coupled device) camera (Andor Technology). For TIRF illumination, a 640-nm (Crystalaser) diode laser was used. A mercury lamp with 560/55 nm filter cube (Nikon) was installed for epifluorescence. Exposure times for TIRF and epifluorescence were set to 20 and 400 ms, respectively. All acquisitions were controlled by Metamorph (Molecular Devices). Single-molecule data were analyzed with a custom-written program in Igor Pro (Wavemetrics) (45). Images were rendered with Fiji (46).

ACKNOWLEDGMENTS. We thank Julie Zorn for her gift of phosphatase. We also thank Jenny J. Lin for the live cell image in Fig. 6, as well as helpful discussion. We thank other members in the J.K. laboratory and the J.T.G. laboratory for stimulating discussions. This work is supported by National Institutes of Health Grant P01 AI091580.

1. Schlessinger J (2000) Cell signaling by receptor tyrosine kinases. *Cell* 103(2):211–225.
2. Groves JT, Kuriyan J (2010) Molecular mechanisms in signal transduction at the membrane. *Nat Struct Mol Biol* 17(6):659–665.
3. Banjade S, Rosen MK (2014) Phase transitions of multivalent proteins can promote clustering of membrane receptors. *eLife* 3:e04123.
4. Janes PW, Nievergall E, Lackmann M (2012) Concepts and consequences of Eph receptor clustering. *Semin Cell Dev Biol* 23(1):43–50.
5. Scott JD, Pawson T (2009) Cell signaling in space and time: Where proteins come together and when they're apart. *Science* 326(5957):1220–1224.
6. Lisabeth EM, Falivelli G, Pasquale EB (2013) Eph receptor signaling and ephrins. *Cold Spring Harb Perspect Biol* 5(9):a009159.
7. Salaita K, et al. (2010) Restriction of receptor movement alters cellular response: Physical force sensing by EphA2. *Science* 327(5971):1380–1385.
8. Lohmüller T, Xu Q, Groves JT (2013) Nanoscale obstacle arrays frustrate transport of EphA2-Ephrin-A1 clusters in cancer cell lines. *Nano Lett* 13(7):3059–3064.
9. Greene AC, et al. (2014) Spatial organization of EphA2 at the cell-cell interface modulates trans-endocytosis of ephrinA1. *Biophys J* 106(10):2196–2205.
10. Dustin ML, Groves JT (2012) Receptor signaling clusters in the immune synapse. *Annu Rev Biophys* 41:543–556.
11. Lillemeier BF, et al. (2010) TCR and Lat are expressed on separate protein islands on T cell membranes and concatenate during activation. *Nat Immunol* 11(1):90–96.
12. Caculitan NG, et al. (2014) Size-based chromatography of signaling clusters in a living cell membrane. *Nano Lett* 14(5):2293–2298.
13. Houtman JCD, et al. (2004) Binding specificity of multiprotein signaling complexes is determined by both cooperative interactions and affinity preferences. *Biochemistry* 43(14):4170–4178.
14. Lowenstein EJ, et al. (1992) The SH2 and SH3 domain-containing protein GRB2 links receptor tyrosine kinases to ras signaling. *Cell* 70(3):431–442.
15. Houtman JCD, et al. (2006) Oligomerization of signaling complexes by the multipoint binding of GRB2 to both LAT and SOS1. *Nat Struct Mol Biol* 13(9):798–805.
16. Nag A, Monine MI, Faeder JR, Goldstein B (2009) Aggregation of membrane proteins by cytosolic cross-linkers: Theory and simulation of the LAT-Grb2-SOS1 system. *Biophys J* 96(7):2604–2623.
17. Kortum RL, et al. (2013) The ability of Sos1 to oligomerize the adaptor protein LAT is separable from its guanine nucleotide exchange activity in vivo. *Sci Signal* 6(301):ra99.
18. Balagopalan L, Kortum RL, Coussens NP, Barr VA, Samelson LE (2015) The linker for activation of T cells (LAT) signaling hub: From signaling complexes to microclusters. *J Biol Chem* 290(44):26422–26429.
19. Li P, et al. (2012) Phase transitions in the assembly of multivalent signalling proteins. *Nature* 483(7389):336–340.
20. Douglass AD, Vale RD (2005) Single-molecule microscopy reveals plasma membrane microdomains created by protein-protein networks that exclude or trap signaling molecules in T cells. *Cell* 121(6):937–950.
21. Zhu M, Janssen E, Zhang W (2003) Minimal requirement of tyrosine residues of linker for activation of T cells in TCR signaling and thymocyte development. *J Immunol* 170(1):325–333.
22. Lin J, Weiss A (2001) Identification of the minimal tyrosine residues required for linker for activation of T cell function. *J Biol Chem* 276(31):29588–29595.
23. O'Donoghue GP, Pielak RM, Smoligovets AA, Lin JJ, Groves JT (2013) Direct single molecule measurement of TCR triggering by agonist pMHC in living primary T cells. *eLife* 2:e00778.
24. Oh D, et al. (2012) Fast rebinding increases dwell time of Src homology 2 (SH2)-containing proteins near the plasma membrane. *Proc Natl Acad Sci USA* 109(35):14024–14029.
25. Gureasko J, et al. (2010) Role of the histone domain in the autoinhibition and activation of the Ras activator Son of Sevenless. *Proc Natl Acad Sci USA* 107(8):3430–3435.
26. Iversen L, et al. (2014) Molecular kinetics. Ras activation by SOS: Allosteric regulation by altered fluctuation dynamics. *Science* 345(6192):50–54.
27. Hopfield JJ (1974) Kinetic proofreading: A new mechanism for reducing errors in biosynthetic processes requiring high specificity. *Proc Natl Acad Sci USA* 71(10):4135–4139.
28. McKeithan TW (1995) Kinetic proofreading in T-cell receptor signal transduction. *Proc Natl Acad Sci USA* 92(11):5042–5046.
29. Nye JA, Groves JT (2008) Kinetic control of histidine-tagged protein surface density on supported lipid bilayers. *Langmuir* 24(8):4145–4149.
30. Lin WC, et al. (2014) H-Ras forms dimers on membrane surfaces via a protein-protein interface. *Proc Natl Acad Sci USA* 111(8):2996–3001.
31. Paz PE, et al. (2001) Mapping the Zap-70 phosphorylation sites on LAT (linker for activation of T cells) required for recruitment and activation of signalling proteins in T cells. *Biochem J* 356(Pt 2):461–471.
32. Rubinstein M, Colby RH (2003) *Polymer Physics* (Oxford Univ. Press, New York).
33. Ensign DL, Pande VS (2010) Bayesian detection of intensity changes in single molecule and molecular dynamics trajectories. *J Phys Chem B* 114(1):280–292.
34. Song L, Hennink EJ, Young IT, Tanke HJ (1995) Photobleaching kinetics of fluorescein in quantitative fluorescence microscopy. *Biophys J* 68(6):2588–2600.
35. Chook YM, Gish GD, Kay CM, Pai EF, Pawson T (1996) The Grb2-mSos1 complex binds phosphopeptides with higher affinity than Grb2. *J Biol Chem* 271(48):30472–30478.
36. Christensen SM, et al. (2016) Monitoring the waiting time sequence of single Ras GTPase activation events using liposome functionalized zero mode waveguides. *Nano Lett* 16(4):2890–2895.
37. Gureasko J, et al. (2008) Membrane-dependent signal integration by the Ras activator Son of sevenless. *Nat Struct Mol Biol* 15(5):452–461.
38. Moffitt JR, Chemla YR, Bustamante C (2010) Methods in statistical kinetics. *Methods Enzymol* 475:221–257.
39. Kou SC, Cherayil BJ, Min W, English BP, Xie XS (2005) Single-molecule Michaelis-Menten equations. *J Phys Chem B* 109(41):19068–19081.
40. Bezanilla F (2005) Voltage-gated ion channels. *IEEE Trans Nanobioscience* 4(1):34–48.
41. Zikherman J, Au-Yeung B (2015) The role of T cell receptor signaling thresholds in guiding T cell fate decisions. *Curr Opin Immunol* 33:43–48.
42. Das J, et al. (2009) Digital signaling and hysteresis characterize ras activation in lymphoid cells. *Cell* 136(2):337–351.
43. Yan Q, et al. (2013) Structural basis for activation of ZAP-70 by phosphorylation of the SH2-kinase linker. *Mol Cell Biol* 33(11):2188–2201.
44. Cordes T, Vogelsang J, Tinnefeld P (2009) On the mechanism of Trolox as antiblinking and antibleaching reagent. *J Am Chem Soc* 131(14):5018–5019.
45. Sergé A, Bertaux N, Rigneault H, Marguet D (2008) Dynamic multiple-target tracing to probe spatiotemporal cartography of cell membranes. *Nat Methods* 5(8):687–694.
46. Schindelin J, et al. (2012) Fiji: An open-source platform for biological-image analysis. *Nat Methods* 9(7):676–682.